Available online at www.sciencedirect.com
SCIENCE DIRECT®
Earth and Planetary Science Letters 236 (2005) 359–373
EPSL
www.elsevier.com/locate/epsl

A new Late Cretaceous paleomagnetic pole for the west of Amuria block (Khurmen Uul, Mongolia)

Fatim Hankard [a,*], Jean-Pascal Cogné [a], Vadim Kravchinsky [a,b]

[a] *Laboratoire de Paléomagnétisme, Institut de Physique du Globe, 4 Place Jussieu, 75252 Paris cedex 05, France*
[b] *Physics Department, University of Alberta, Edmonton AB, Canada T6G 2J1*

Received 27 October 2004; received in revised form 13 April 2005; accepted 29 May 2005
Available online 28 June 2005
Editor: R.D. van der Hilst

Abstract

We present new paleomagnetic results obtained at ten sampling sites from six Upper Cretaceous (92 ± 4 Ma) basaltic lava flows from the westernmost part of Amuria block. The samples were collected in 1999 in the Khurmen Uul region (44.0°N, 103.0°E), Gobi desert (S. Mongolia). Stepwise thermal demagnetization isolated a high temperature component (HTC) carried by magnetite. Five out of ten sites exhibit anomalously high Koenigsberger ratios and low inclinations, which likely resulted from lightning remagnetization. However, three of these sites were only partially remagnetized, allowing us to use remagnetization great-circles to help determine a characteristic magnetization direction for this formation. HTC directions of the eight remaining sites from six distinct flows all possess normal polarity and exhibit better clustering after tilt correction of the flows (ks/kg = 129.3 / 36.6, $n = 6$). This clustering is ascertained by a positive fold test at the specimen scale within a single flow. We therefore propose that the tilt-corrected HTC represents a primary magnetization. The paleopole computed from the six lava flows HTC mean directions lies at $\lambda = 71.5°$N, $\phi = 227.2°$E (dp/dm = 5.6° / 8.2°). We discuss the possibility that our pole might not have completely averaged paleosecular variation, because it is based on only 6 independent flows. Finally, this pole is far-sided with respect to the 90 Ma reference pole of Eurasia APWP ($\Delta\lambda = 10.2° \pm 6.1°$), but it is consistent, albeit somewhat far-sided too, with other coeval paleopoles from Amuria, and east China.

Keywords: paleomagnetism; tectonics; Central Asia; Mongolia; Gobi Desert; Cretaceous effusives

1. Introduction

Central Asia consists of a mosaic of blocks, which began accreting in the Early Paleozoic. The configuration of this continent has been profoundly modified since the India–Asia collision in the Eocene (45–50 Ma) [1–4]. This vast territory has become the location of the highest mountain ranges and most extended and elevated plateaus in the world.

Over the last few decades, great efforts in paleomagnetic data acquisition have been undertaken in order to better understand the geodynamic processes implied in a

* Corresponding author. Tel.: +33 1 44 27 68 70; fax: +33 44 27 74 63.
E-mail address: hankard@ipgp.jussieu.fr (F. Hankard).

0012-821X/$ - see front matter © 2005 Elsevier B.V. All rights reserved.
doi:10.1016/j.epsl.2005.05.033

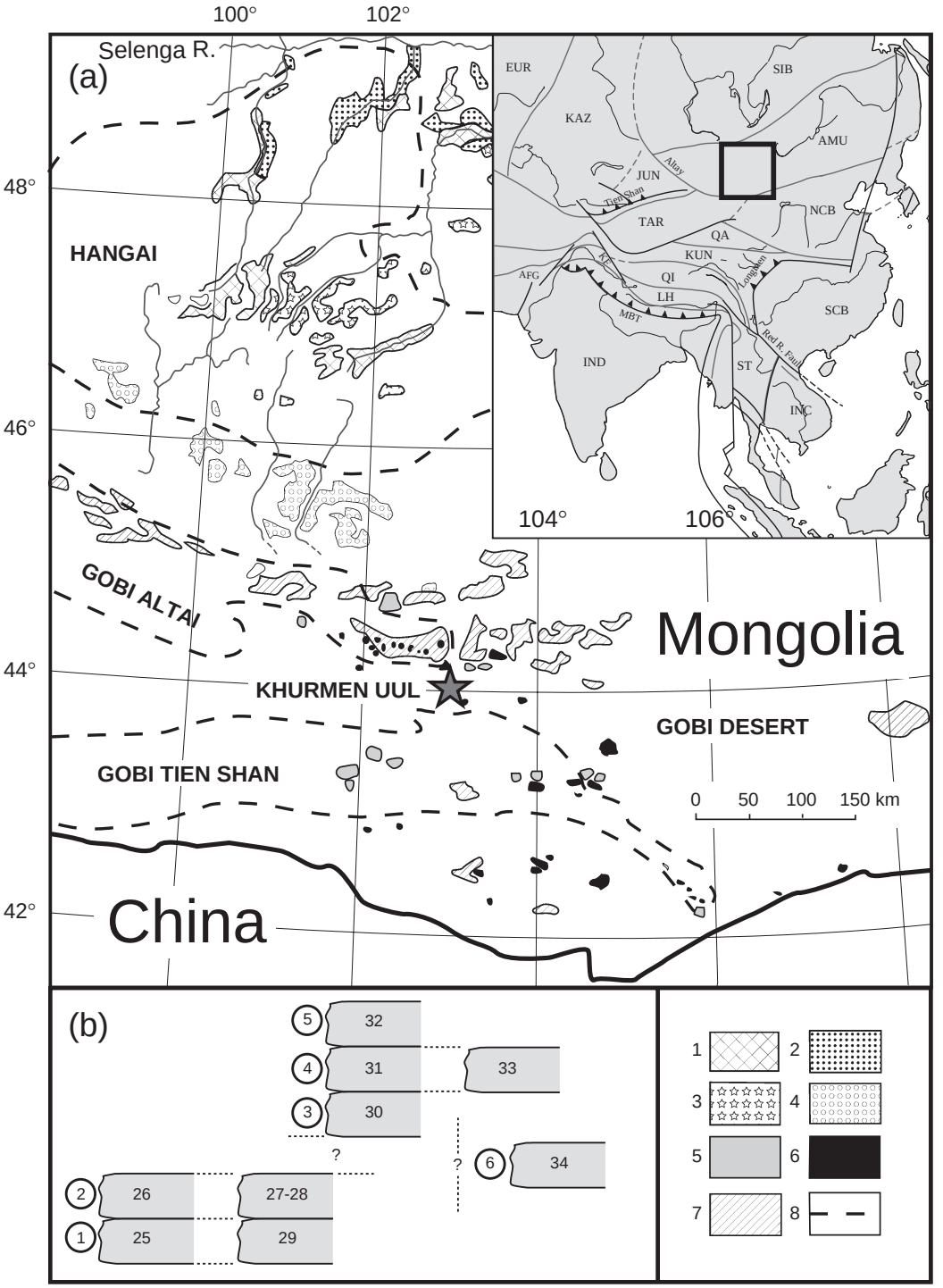
100°
102°
Selenga R.
(a)
48°
46°
44°
42°
HANGAI
GOBI ALTAI
KHURMEN UUL
GOBI TIEN SHAN
GOBI DESERT
Mongolia
China
0 50 100 150 km
EUR
SIB
KAZ
AMU
JUN
Altay
Tien Shan
TAR
NCB
QA
KUN
Kunlun
AFG
QI
LH
MBT
Red R. Fault
SCB
IND
ST
INC
104°
106°
(b)
5
32
4
31
33
3
30
?
?
6
34
2
26
27-28
1
25
29
1
2
3
4
5
6
7
8

continental collision. In effect, because all the blocks constituting the Asian continent are thought to have been accreted by the Cretaceous, except for India, rocks of Cretaceous age have been the main focus of most studies. Therefore, the Cretaceous is the period for which the most reliable and consistent paleomagnetic database exists for almost each block (North China block or NCB, South China block or SCB, Tibetan blocks, Tarim, Jungar, Qaidam, Amuria, Siberia), [5–10]. Analyses and interpretations of this database have allowed several authors [5,11–14] to propose paleogeographic reconstructions of the Asian mosaic prior to the collision.

Concerning Amuria, NCB, SCB and Siberia, numerous paleomagnetic studies were undertaken in the region [6–8,15–21]. They show that (1) NCB accreted to Amuria by the Late Carboniferous, (2) SCB then sutured with NCB around the Middle to Late Jurassic, and (3) finally, the Mongol–Okhotsk Ocean between Amuria and Siberia closed by the Late Jurassic. These studies also demonstrated the lack of significant post-Cretaceous latitudinal relative changes of this assemblage since then. On the other hand, there was significant northward convergence of Tarim Block with respect to Siberia since the Cretaceous, which led Enkin et al. [5] and Chen et al. [10] to propose the possible existence of a tectonic discontinuity between Tarim and NCB which could be located near 95–100°E longitude, between NCB, SCB, Amuria to the east and Tarim to the west. Yet, there is no geological evidence for such a major tectonic discontinuity.

In order to better constrain the paleolatitude of Amuria and hopefully the location of the tectonic discontinuity zone, we have acquired new paleomagnetic data from an Upper Cretaceous basaltic formation from Khurmen Uul (44.0°N, 103.0°E), in the Gobi Desert (Mongolia). Samples were collected during a field trip in 1999. In effect, the bulk of paleomagnetic data available so far come from the stable NCB and SCB, located east of the discontinuity, and Tarim to the west of it. This is why we selected a sampling area in Amuria, which is located near the northward extension of the potential NS trending discontinuity zone.

2. Geology and paleomagnetic sampling

Following Zonenshain [22], the Amuria microcontinent consists of a number of lithospheric blocks (Hangai, Hentei, Central Mongolia, Argun, Khingan-Bureya), which accreted together in the early Paleozoic. The Amuria Block constitutes the eastern part of the Asian continent, together with Siberia, NCB and SCB. Its topography results from the India–Eurasia collision in the Eocene [2,23]. It is characterized both by the Mongolian plateau, consisting of the Hangai and Hentei Domes [23,24], and the Gobi Altai and Gobi Desert which bound Amuria to the south (Fig. 1a). The Mongolian plateau (2500 × 700 km), with an average altitude of 2000 m, occupies most of Mongolia and is bounded to the north by the Transbaikalia–Amur region of southeast Siberia.

The Gobi Altai is an extension of the Altai mountain ranges to the southeast (Fig. 1a). This region consists of topographically discontinuous ranges, with peaks averaging 2000–3000 m in elevation [23,25–28]. To the east of Gobi Altai and Gobi Tien Shan, the Gobi Desert extends along the border of southern Mongolia.

The basement rocks of the eastern Gobi Altai consist of discontinuously exposed Paleozoic low-grade metasedimentary rocks, volcaniclastic sedimentary rocks, carbonates and isolated felsic intrusions, which are thought to represent arc basement, arc-derived sediment and continental platform material [29,30]. Several authors [31–33] have reported that Late Jurassic and Cretaceous continent-derived clastic and local volcanic rocks, deposited during a period of intraplate extension and volcanism, lie unconformably on deformed Paleozoic and early Mesozoic rocks. To the southeast of Gobi Altai begins the domain of the Gobi Desert, where Cretaceous and Paleocene rocks

Fig. 1. (a) Simplified map of Late Mesozoic–Cenozoic volcanic fields in Southern and Central Mongolia (after Kovalenko et al., [53]). Star: Khurmen Uul locality; (1) Pleistocene–Holocene; (2) Pliocene; (3) Middle Miocene; (4) Late Oligocene and early Miocene; (5) Early Cenozoic; (6) Late Cretaceous; (7) Late Jurassic and Early Cretaceous; (8) Boundaries of highlands and ranges; inset: situation map of Fig. 1a in Asia, with main blocks indicated (AMU: Amuria, AFG: Afghanistan, EUR: Eurasia main plate, INC: Indochina, IND: India JUN: Junggar, KAZ: Khazakhstan, KUN: Kunlun, LH: Lhasa, MBT: Main Boundary Thrust, NCB: North China Block, QA: Qaidam, QI: Qiangtang, SCB: South China Block, SIB: Siberia, ST: Shantä, TAR: Tarim). (b) Sketch of relative positions of flows and sites sampled at Khurmen Uul; circled numbers 1 to 6 are flows, numbers 25 to 34 are sampling sites.

are widely distributed (Fig. 1a). Cretaceous volcanism is limited to distinct and widely separated localities where thin andesitic to basaltic lava flows and some locally thick tuffs and volcaniclastics outcrop [34].

Our sampling sites are located at the southeasternmost end of the Gobi Altai, on the Khurmen Uul ridges (44.0°N–103.0°E; Fig. 1a). Ten Upper Cretaceous sites were sampled from a basaltic formation made of ~2–3 m thick flows. A radiometric K/Ar age of 92 ± 4 Ma has been obtained [35]. According to field observations, and despite discontinuous outcropping conditions, we think we have sampled six distinct flows. The relationships between sites and flows are schematically illustrated in Fig. 1b. Sites 25 and 29 were drilled in the lowermost flow and sites 26, 27 and 28 from the immediately overlying flow. They are followed by a series of 3 flows sampled as sites 30, 31 and 32. Site 33 was sampled in the same flow as site 31. Finally, site 34 was sampled in an isolated flow. Its relative position is difficult to ascertain, but we assume that it is a different flow. The tilt of the flows was measured in the field, however poor outcrop conditions did not allow clarifying the stratigraphic contact between the flows and the underlying sediments. Eight to ten cores per site were collected with a gasoline powered portable drill. Because of rainy weather, all the cores were oriented using only magnetic compass. Accordingly, field measurements were corrected for local magnetic declination ($-1.6°$) using the IGRF 1995 coefficients and their time derivatives.

3. Paleomagnetic analysis and results

Magnetic measurements and demagnetization procedures were performed in the magnetically shielded room of the Paleomagnetic laboratory at the Institut de Physique du Globe (IPG) in Paris and St. Maur. Remanent magnetization measurements were carried out using an Agico JR5 spinner magnetometer. All samples were thermally demagnetized over 19 temperature steps up to 590–600 °C within a nearly zero field laboratory built-furnace. During thermal demagnetization, sample orientation was successively inverted about the z-axis in order to detect any systematic magnetization that could have resulted from the small ~10 nT residual magnetic field in the furnace.

In order to identify of the magnetic carriers, acquisition of isothermal remanent magnetization (IRM) was measured on one specimen per site. Hysteresis loops were also determined on a few specimens, using a laboratory-made translation inductometer. Curie points were determined using an Agico Kappa-bridge KLY-3 and a CS-2 high temperature susceptibility meters. Demagnetization results were plotted on orthogonal vector diagrams, [36] and also on equal-area projections. Magnetization components were determined by principal component analysis [37]. Site-mean directions were calculated using Fisher statistics [38], or using the statistics of McFadden and McElhinny [39] for combined great-circle and vector populations. Finally, we attempted to better define the tilt of flows by measuring the anisotropy of magnetic susceptibility (AMS) of a few specimens. Unfortunately, AMS appeared very weak, with k1/k3 ratios of ~1.005–1.015, precluding any such determination. All interpretations and data processing were carried out using the PaleoMac software [40].

NRM intensities of the basaltic lava flows (Tables 1 and 2) fall into two distinct groups. In the first group (sites 25, 30, 31, 33 and 34), NRM ranges from 0.08 A/

Table 1
Site-mean paleomagnetic directions of lightning IRM from Khurmen Uul Upper Cretaceous basalts

Sites	Strike/Dip (°)	n/N	Dg (°)	Ig (°)	Ds (°)	Is (°)	k	α_{95} (°)	NRM	Q	(n*)
26	353.4/12.0	10/10	144.2	−19.5	148.5	−25.3	252.2	3.5	30.0 ± 14.0	176.7	4
27	358.4/17.0	9/10	7.4	16.1	11.9	13.2	15.1	13.7	14.0 ± 13.0	91.7	4
28	358.4/17.0	8/10	165.6	6.7	164.3	2.3	7.8	21.1	13.6 ± 11.8	51.0	4
29	358.4/17.0	8/10	318.1	−2.8	318.7	8.6	22.9	11.8	78.0 ± 35.0	337.0	4
32	310.8/23.0	9/12	336.3	25.6	343.9	14.8	24.7	10.6	4.2 ± 1.8	21.0	6

Strike/Dip of the flows; n/N: number of samples used in the statistics/number of demagnetized specimens; Dg/Ig (Ds/Is), declination and inclination in geographic coordinates, in situ (stratigraphic coordinates, after tilt-correction); k, α_{95}, parameters of Fisher [38] statistics; NRM: mean NRM intensities for each sampling site; Q: Koenigsberger ratios [41]; (n*): number of specimens used in the Koenigsberger ratios.

Table 2
Site-mean paleomagnetic directions for the high temperature component (HTC) from Khurmen Uul Upper Cretaceous basalts

Flows	Sites	Strike/Dip (°)	Type	*n*/*N*	Dg (°)	Ig (°)	Ds (°)	Is (°)	k	α_{95}(°)	NRM	*Q*	(*n**)
1	25	353.4/12	HT	10/10	4.1	55.7	19.7	51.8	165.4	4	0.15 ± 0.05	3.4	4
		26:353.4/12	GC	5/20	7.1	59.3	–	–	–	5.4	30.0 ± 14.0	176.7 (26)	4
2	26–27	27:358.4/17	GC	5/20	–	–	29.7	51.1	–	5	14.0 ± 13.0	91.7 (27)	3
3	30	310.8/23	HT	8/8	6.8	71.2	25.3	50.3	46.4	8.2	0.4 ± 0.05	2.1	4
		31:310.8/23	HT	15/15	338.8	52.4	–	–	38.1	6.3	0.78 ± 0.10	5.3 (31)	5
4	31–33	33:8.4/19	HT	15/15	–	–	0.8	47.9	204.8	2.7	0.55 ± 0.07	2.8 (33)	4
5	32	310.8/23	GC	9/12	61.9	−8.4	64.8	−29.9	α_{95x}=1.3	α_{95y}=3.7	4.2 ± 1.8	21.0	6
6	34	173.4/12	HT	10/10	27.5	48.9	14	54.4	398	2.4	0.87 ± 0.07	4.0	5
Mean				6/6	3.9	60.5	–	–	36.6	11.4	–	–	
				6/6	–	–	18	51.4	129.3	6	–	–	

HT: high temperature magnetization components; GC: remagnetization great circle; Strike/Dip of the flows; *n*/*N*: number of samples used in the statistics/number of demagnetized specimens; Dg/Ig (Ds/Is), declination and inclination in geographic coordinates, in situ (stratigraphic coordinates, after tilt-correction); k, α_{95}, parameters of Fisher [38] statistics; NRM: mean NRM intensities in Am-1; Q: Koenigsberger ratios [41]. Data displayed for site 32, in italics, are the average normals to remagnetization great-circles computed using the bivariate statistics of Le Goff [42]; (*n**): number of specimens used in the Koenigsberger ratios.

m to 1 A/m with a mean value at 0.56 ± 0.28 A/m (*n*=43). The second group (sites 26 to 29, and 32) exhibits much higher values, ranging from 1 to 89 A/m (up to 120 A/m for 3 specimens), with a mean value at 27.0 ± 31.8 A/m (*n*=52). The mean Koenigsberger ratios (Q) [41] for all sites are listed in Tables 1 and 2, where the second group of sites exhibits anomalously high values.

Thermal demagnetization isolated a high temperature component (HTC) in most of the samples. In some samples, this HTC, which was removed between 250–300 °C and 590 °C (Fig. 2a), follows a low temperature component (LTC) unblocked between room temperature and 200–250 °C. In most sites, including those with high NRM and Koenigsberger ratios (Fig. 2b), HTC converges toward the origin of orthogonal plots. However such is not the case in sites 25 and 32 (Fig. 3), where LTC and HTC were poorly separated, leading to a great-circle path of points. In site 25 (Fig. 3a), the HTC was well separated in only three out of ten samples, the other ones display only great circle trajectories. For this reason, the site-mean direction of site 25 was computed using the combined average of McFadden and McElhinny [39]. In contrast, demagnetization paths never converged towards the origin in specimens from site 32 (Fig. 3b). In this site, we computed an average remagnetization great-circle, using the bivariate statistics of Le Goff [42]. Although most of the specimens from sites 26 and 27, with high Koenigsberger ratios, exhibit HTC which converge towards the origin of orthogonal plots, we isolated two remagnetization great-circles in site 26 (Fig. 4a), and three in site 27 (Fig. 4b). Their significances are discussed below.

The maximum unblocking temperature of 590 °C indicates that the HTC is carried by magnetite. This observation is confirmed by magnetic mineralogy experiments. Both IRM acquisition curves (Fig. 5a) and hysteresis loops (Fig. 5b) show that saturation is achieved by 0.3 T. The high-temperature susceptibility measurements (Fig. 5c) display a sharp drop in magnetic susceptibility at about 580 °C, the Curie point of magnetite. The same experiments were conducted on one specimen from each site, and gave similar results for all sites, including those with high NRM intensities and Koenigsberger ratios. The similarities in the magnetic mineralogy among the different sites are illustrated by the Day et al. [43] plot of Fig. 5d, where all sites cluster in the pseudo-single domain (PSD) zone with no difference between the sites with high NRM intensities and the others. The high Jrs/Js value of site 33 specimen may denote a higher (lower) volume fraction of single domain (SD) (multi-domain (MD)) magnetite [44], but is not correlated to NRM intensity (Table 2).

The interpretation of the HTC is not straightforward. In the following, we first analyse HTC site-mean directions from sites 26 to 29 and 32, which exhibit high NRM and Koenigsberger ratios. Although they are generally well-behaved during demagnetization, the within-site mean directions of HTC from this group of sites (Table 1, Fig. 6) show a large scatter, mainly in

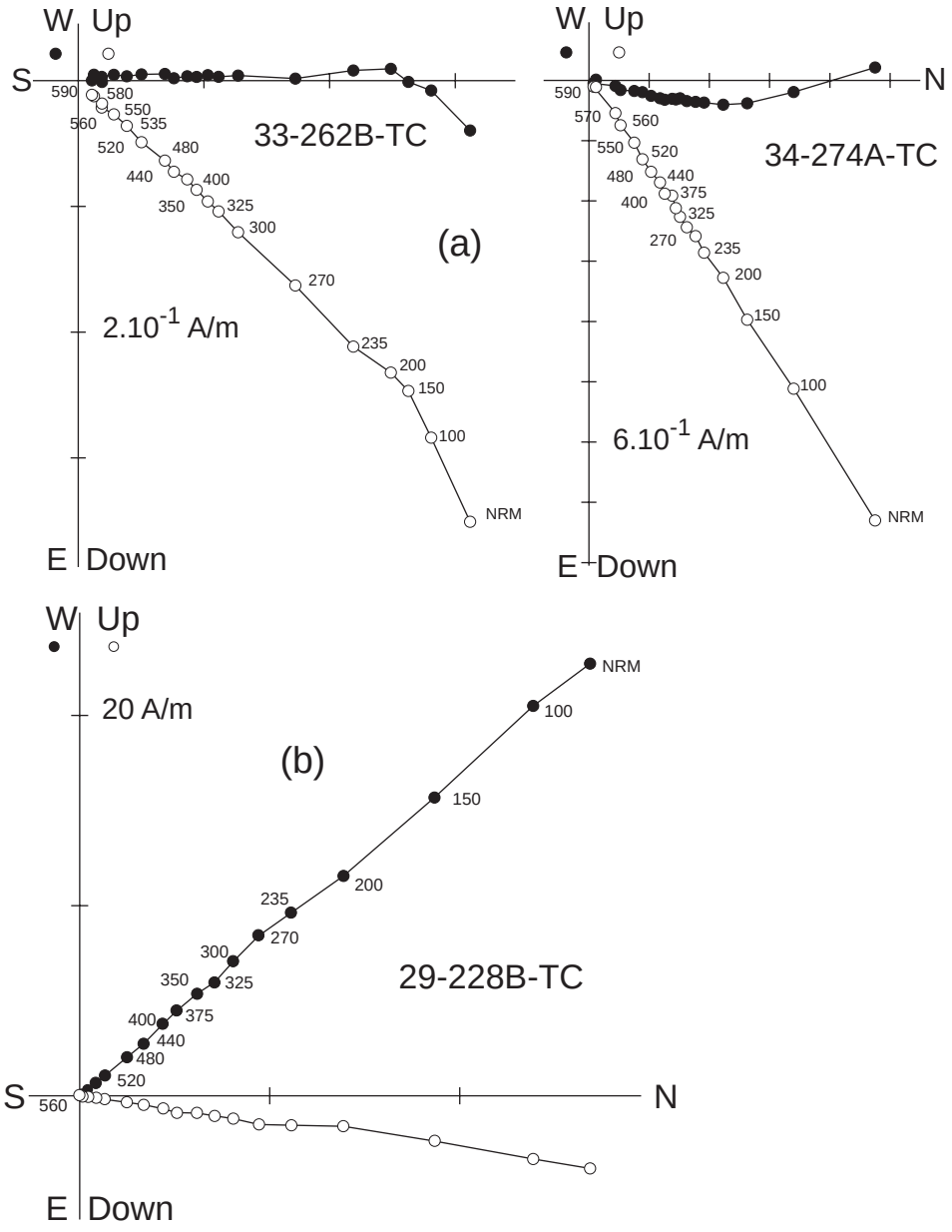

Fig. 2. Orthogonal vector plots [36] of thermal demagnetization results in tilt-corrected coordinates; solid (open) symbols are projections onto the horizontal (vertical) plane; temperature steps are indicated in °C. (a) Typical examples from sites 33 and 34 with low NRM intensities; (b) a typical example from site 29 with high NRM intensities.

declination, whereas inclinations are always very low, close to the horizontal plane in tilt-corrected coordinates. Altogether, strong NRM intensities, high Koenigsberger ratios, identical magnetic properties and magnetic vectors within the flow plane lead us to conclude that the HTC from these sites might be an isothermal remanent magnetization (IRM) due to lightning having struck the outcrops.

However, although the lightning IRM is the only magnetization component we could isolate in sites 28

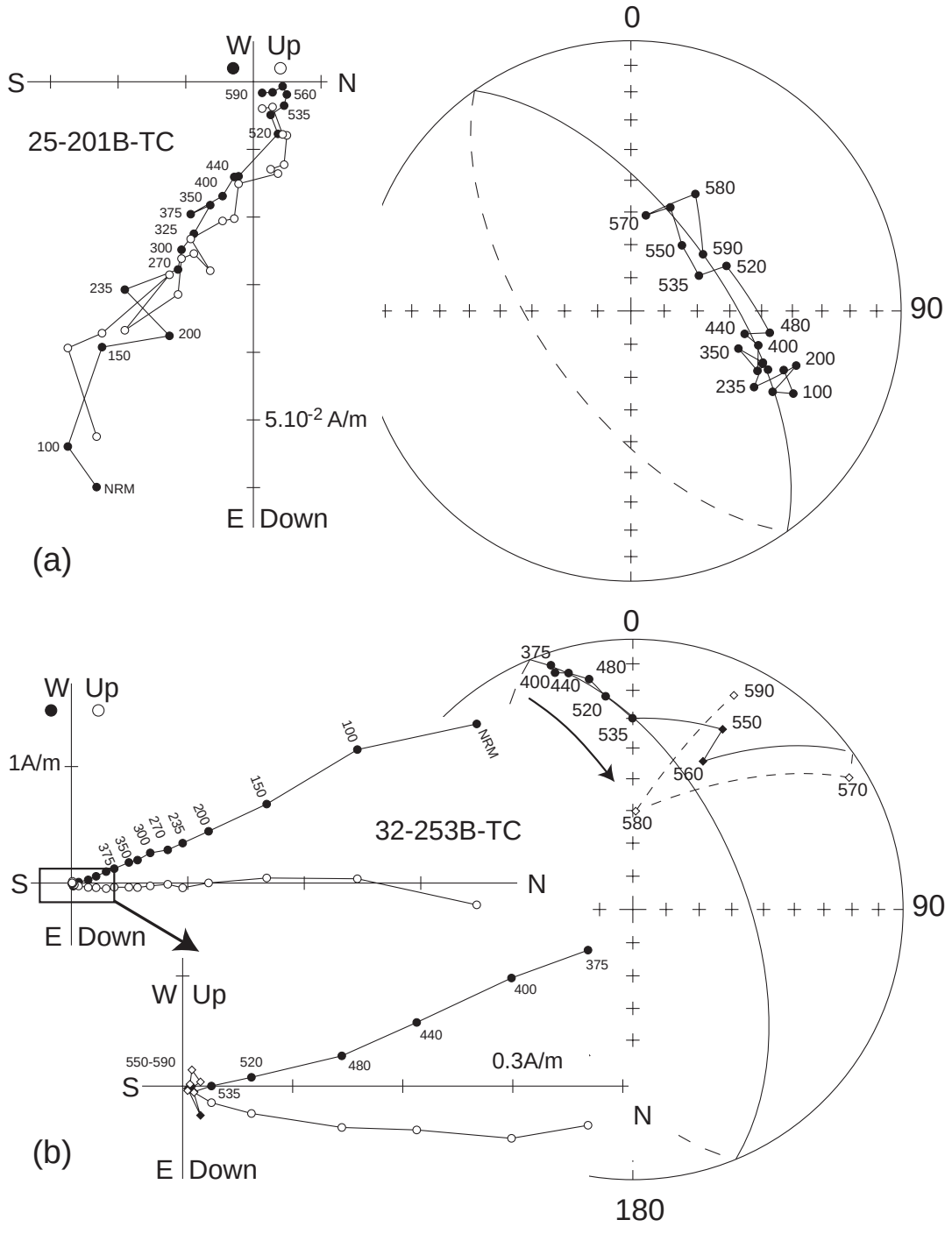

Fig. 3. (a) Orthogonal vector plot and stereonet of thermal demagnetization of a specimen from site 25 showing a great-circle path during demagnetization. (b) Left : orthogonal plot of a specimen from site 32 with an enlargement above 375 °C; albeit straight, the trend does not converge toward the origin, defining a great-circle path (right), from a shallow NNW component to a steeper one. In this example, points above 535 °C (diamonds) are excluded from the great-circle fit. Same conventions as in Fig. 2.

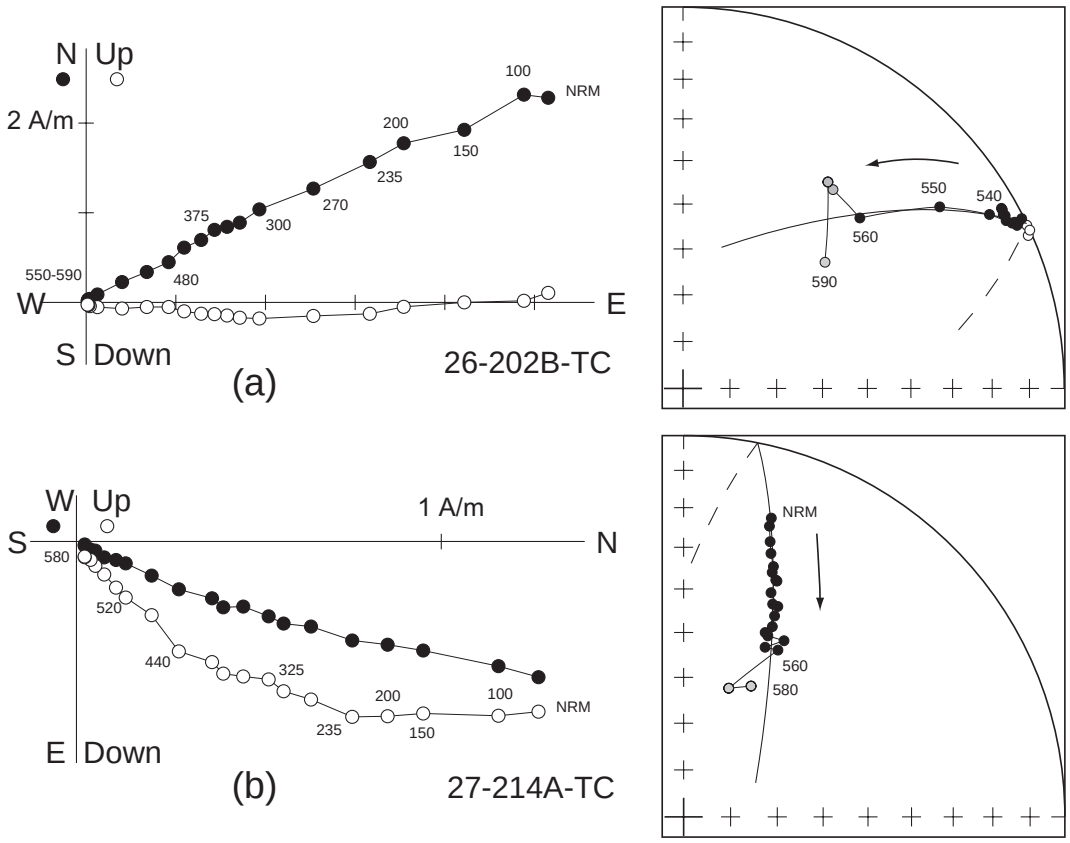

Fig. 4. Orthogonal vector plot and stereonet of thermal demagnetizations of a specimen from site 26 (a) and 27 (b) showing a great-circle path during demagnetization (see text). Same conventions as in Fig. 2.

and 29 (e.g. specimen 29-282B, Fig. 2a), the lightning induced remagnetization did not completely overprint the entire unblocking spectra of some samples in the other sites. In effect, although specimens from site 32 exhibit a well-defined linear demagnetization path (Fig. 3b), which allows defining the IRM component, they also show a systematic great-circle evolution during demagnetization. It was also possible to recover such great-circles in a few specimens from sites 26 and 27 (Fig. 4). Assuming that these great-circles result from the evolution of magnetization between the IRM and a possibly primary magnetization during thermal demagnetization, we attempt to use them in determining the characteristic magnetization of these flows. The great-circles from sites 26 and 27, which based on field observations are two outcrops of the same flow (flow 2, see Fig. 1b), corroborate this analysis: whereas great-circles from both sites 26 and 27 carry a strong IRM, they crosscut each other at a single point (Fig. 7a), which could well be the common "pre-lightning" magnetization component of this flow. A similar analysis is not possible for the remagnetized site 32 (Fig. 7b), since it is the site representative of flow unit 5. Therefore, we will compare the average great-circle of site 32 to the average flow-mean directions from the other sites.

HTC directions from the 5 remaining sites (25, 30, 31, 33 and 34) and great-circles from sites 26, 27 and 32 have been averaged at the flow level in the following way (Table 2, Fig. 8a): flows 1, 3 and 6 (*F1, F3 and F6* in Fig. 1b) are characterized by the HTC averages of sites 25, 30 and 34 respectively. The HTC direction of flow 4 (F4) is computed from site 31 and 33 data; the (hopefully) characteristic magnetization of flow 2 (F2)

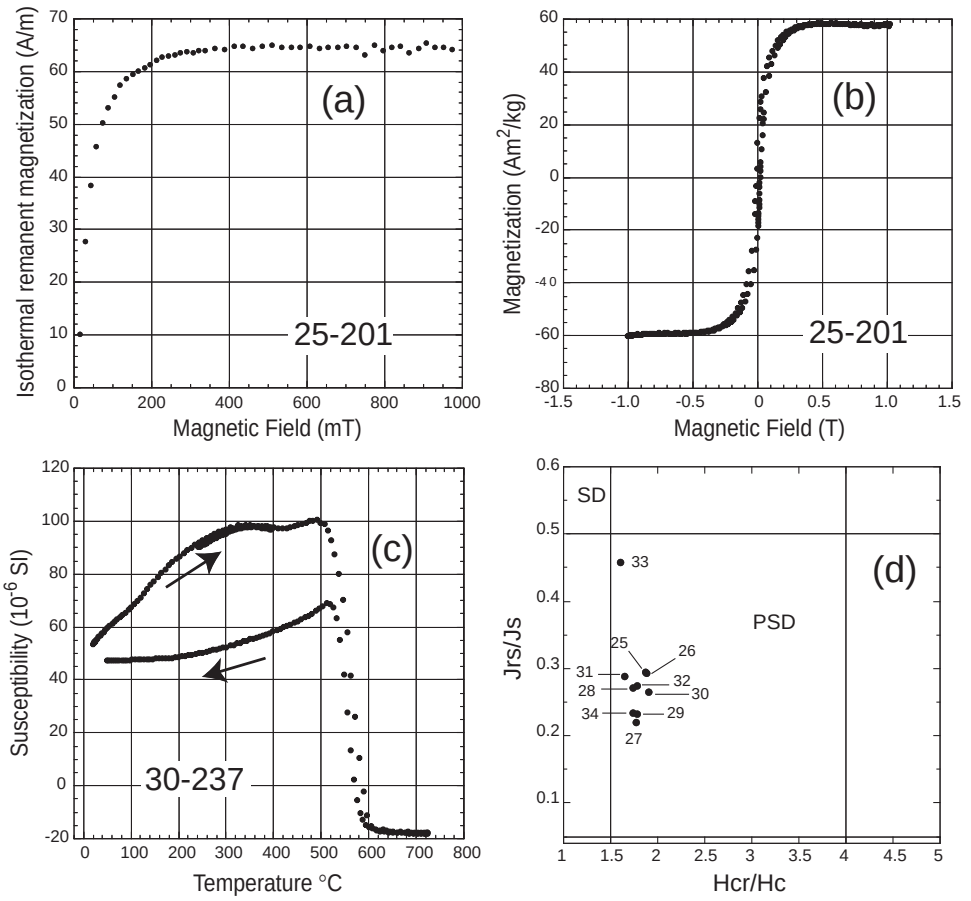

Fig. 5. (a) Isothermal remanent magnetization (IRM) acquisition in fields up to 1T showing the presence of low-coercivity magnetic mineral; magnetizing field in milliTesla (mT). (b) Hysteresis loop after the correction of paramagnetic component showing the presence of low-coercivity magnetic mineral; field in Tesla (T). (c) Susceptibility curve versus temperature showing a Curie point at 580 °C. Temperatures are indicated in °C. (d) Day et al. [43] plot showing all samples plot in the pseudo-single domain (PSD) grain size area; numbers 25 to 34 are the sampling sites.

is defined by the intersection of sites 26 and 27 great-circles as discussed above. Finally, flow 5 (F5) is constrained only by the average great-circle of site 32.

First, we note that the average great-circle of site 32 (flow 5) consistently passes through the vector population of the other flows. We therefore computed the formation mean direction by using the combined average of McFadden and McElhinny [39], including this great-circle (Fig. 8a). Second, directions of the six distinct flows obviously cluster upon untilting (Table 2, Fig. 8a). The tilt-corrected volcanic formation combined mean direction is Ds=18.0°, Is=51.4° (ks=129.3, α_{95}=6.0°, n=6 flows). The precision parameter k increases from kg=36.6 to ks=129.3 upon untilting. With ks/kg=3.533, this increase is significant at the 95% probability level (critical value: 2.970) for n=6, but not at the 99% probability level (critical value: 4.850). If we now exclude the great-circle of site 32, the fold test of McFadden [45] is inconclusive at both the 95% and 99% probability levels for n=5. However, a stronger test is provided by the single flow 4, which has been sampled at two sites (31 and 33) with different tilt attitudes. In this flow, the tilt-correction undoubtely induces a clustering of HTCs from both sites (Table 2, Fig. 8b), which is statistically supported by an increase of the k parameter from 38.1 to 204.8 (n=15 specimens) and a significant positive fold test [45] at both the 95% and 99% probability levels. We finally note that all specimens exhibit normal polarity magnetizations, which is consistent with an age of the formation

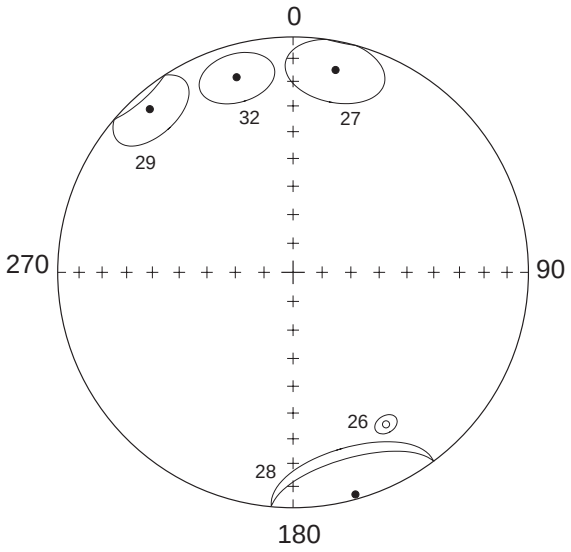

Fig. 6. Equal-area projections of the characteristic IRM site-mean directions for sites having high NRM intensities and Koenigsberger ratios [41], with their α_{95} circles of confidence in tilt-corrected coordinates; solid (open) symbols: positive, downward (negative, upward) inclinations.

within the Cretaceous Long Normal Superchron. Altogether, we conclude that although its In Situ average (Fig. 8a) contains the present-day dipole field axis and the IGRF field directions, the tilt-corrected HTC, which is carried by magnetite, is likely the primary Late Cretaceous magnetization of these basaltic lava flows. The failure of the fold test at the formation level is thought to arise from both the small number of flows and the weak tilt of the flows (Table 2).

4. Discussion

Assuming we have recovered the primary magnetization carried by magnetite, we computed a paleopole from the combined (HTC and great circles) mean direction in tilt-corrected coordinates. This paleopole (Table 2) lies at $\lambda = 71.5°$N, $\phi = 227.2°$E (dp/dm = 5.6°/8.2°) yielding a Late Cretaceous paleolatitude of $32.0° \pm 5.6°$ for the Khurmen Uul location. The Late Cretaceous Khurmen Uul pole appears far-sided with respect to the 90 Ma pole of the reference APWP for Eurasia [46] (Fig. 9a). The discrepancy between the two poles, computed following Coe et al. [47], and as underlined by the difference between the small circles centered on site location, amounts to $\Delta\lambda = 10.2 \pm 6.1°$ in paleolatitude and to an insignificant local rotation of $7.6 \pm 9.6°$. At face value, our result would suggest some 1130 ± 670 km of northward convergence of our sampling region with Siberia, consistent with the shortening between Tarim and Siberia, as proposed by

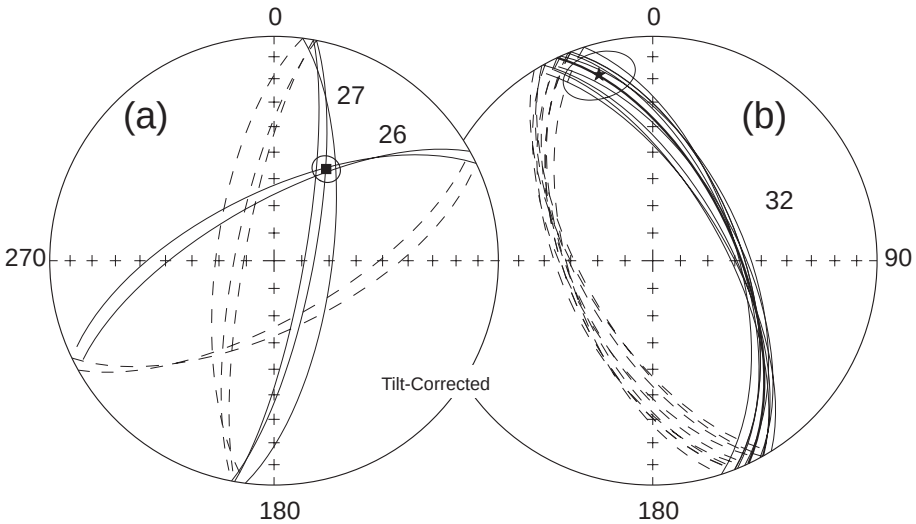

Fig. 7. (a) Equal-area projection of sites 26 and 27 remagnetization great-circles and their intersection (black square with its α_{95} confidence area) in tilt-corrected coordinates; solid (dashed) lines: projection in the lower (upper) hemisphere. (b) Equal-area projection of site 32 remagnetization great-circles; bold line: average great-circle; star with α_{95} area: mean lightning remagnetization component of site 32 (see text and Fig. 6).

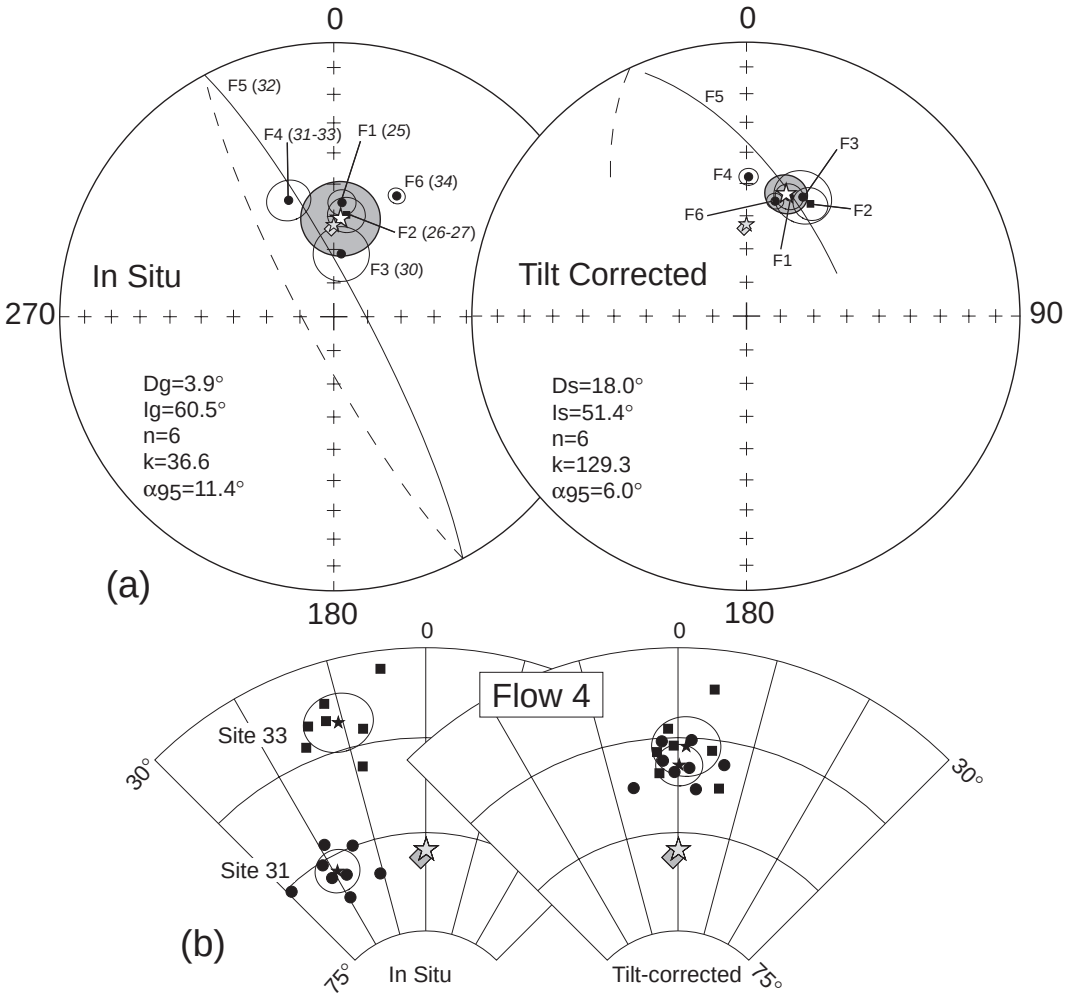

Fig. 8. (a) Equal-area projections of HTC site-mean directions from sites with low Koenigsberger ratios [41] and/or remagnetization great-circles (see text), with their α_{95} circles of confidence before (left) and after (right) tilt-correction; white stars with shaded α_{95} areas: overall-mean directions (lower hemisphere); F1 to F6: flows with their corresponding sites numbers between parenthesis and in italic. (b) Equal-area projections of specimens HTC of sites 31 and 33 from Flow 4, before (left) and after (right) tilt-correction. Light grey diamond and star in (a) and (b): IGRF and axial geocentric dipole field directions. Same conventions as in Figs. 6 and 7.

Chen et al. [10]. However, because average paleopoles from Amuria and China (NCB, SCB and ELKB) do not show a large offset with respect to the reference APWP, a ~1000 km convergence between Khurmen Uul area and Siberia would imply a relative movement between our sampling area (western Amuria) and the rest of Amuria and China to the east. This interpretation is hardly supported by any geological evidence north of Amuria that could have absorbed such a motion. In effect, maps of Moho depth from Zorin [48] show that crustal thickness between our sampling locality and Lake Baikal could result from a maximum 250–300 km of continental shortening. Based on the 2000 m average elevation of the Mongolian Plateau, its extent (2500×700 km) and isostasy, one obtains a similar amount of crustal shortening (~220 km). Finally, according to Zorin [48], this crustal thickening is likely due to Mongol–Okhotsk collision in the Middle-Late Jurassic. Altogether, this shortening is not likely to have been caused by Tertiary tectonic movements due to India collision with Eurasia, and does not solve the discrepancy of our pole with the Eurasia APWP.

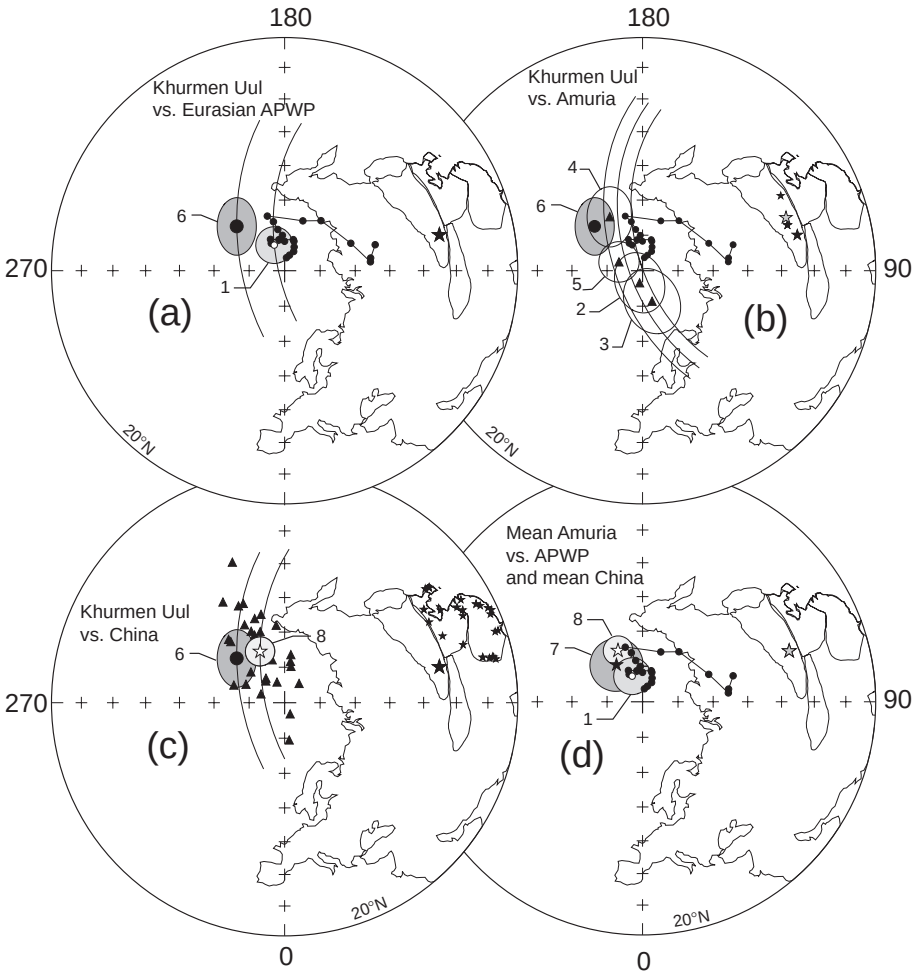

Fig. 9. Equal-area projections of paleomagnetic poles in the northern Earth hemisphere; (a) Late Cretaceous paleomagnetic pole from Khurmen Uul, Mongolia (solid dot with dark grey ellipse of confidence); Small dots: APWP poles for Eurasia [46]; white dot with light grey A_{95} area of confidence: 90 Ma reference pole from the APWP; solid lines: small-circles passing through the poles and centered on the Khurmen Uul average site locations; (b) Khurmen Uul pole compared to other Cretaceous poles from Amuria (solid triangles labelled 2 to 5); lines are the average small-circle and its 95% area of confidence passing through the Amuria poles, excluding Khurmen Uul; (c) Khurmen Uul pole compared to Cretaceous poles from NCB, SCB and Eastern Liaoning-Korea Block (ELKB) (solid triangles) and their average (white star with light grey ellipse of confidence); for clarity, ellipses of confidence of individual poles have not been drawn; (d) Mean paleomagnetic pole for Amuria (solid star with dark grey A_{95} area of confidence) compared to both 90 Ma reference pole from APWP (white dot with light grey ellipse of confidence) and mean paleomagnetic pole for China (white star with grey ellipse of confidence); black stars: sites location; large grey star in (b) and (d): average site locations for Amuria block. Labels 1 to 8 in (a), (b), (c) and (d) refer to pole Id of Table 3.

Since our average paleomagnetic direction is based on only 8 independent sites from 6 flows, we have tested the angular dispersion of the virtual geomagnetic poles (VGP) computed from the 5 flows exhibiting a HTC direction, excluding the site 32 great-circle result. We obtain a VGP scatter of 8.9°, somewhat smaller than the 12–15° VGP scatter predicted by McFadden et al. [49] at 30–40° latitude for the 80–110 Ma period. This suggests that our data may not have fully averaged out secular variation at the time of flow emplacement. If we now do a comparison with other poles from Amuria (Fig. 9b), and east Chinese poles from NCB, SCB and ELKB (Fig. 9c), we note that our pole is not inconsistent with these popula-

Table 3
Selected Cretaceous paleomagnetic poles from Asia and Eurasia reference

Block	Id	Name	Age	Slat	Slon	Plat	Plon	dp/dm or A_{95}	*n*	References
Eurasia APWP	1.	–	90 Ma			82.2	202.1	5.2	13L	[46]
Amuria	2.	Chulut Tsagan Del # 12	K	46.1	107.5	86.5	346.5	6.9/8.8	17 s	[50]
	3.	Chulut Tsagan Del # 13	K	46.1	107.5	81.0	17.2	7.7/9.7	19 s	[50]
	4.	Gobi # 14	K	46.1	107.5	72.1	211.3	6.4/8.6	30 s	[50]
	5.	Inner Mongolia	K	44.5	118.5	82.9	249.5	5.7/5.7	6 S	[16]
	6.	Khurmen Uul	K_2	44.0	103.0	71.5	227.2	5.6/8.2	8 S	This study
	7.	Amuria Mean	K			77.3	215.2	7.5	5 L	
NCB+SCB+ELKB	8.	–	Mean K			73.2	205.6	4.1	29 L	[54]

Slat, Slon (Plat, Plon): Latitude and longitude of sites (poles); dp/dm: half-angles of the ellipse of confidence; A95: radius of 95% cone of confidence; *n*: number of localities; L: locality, S: sites, s: specimens. Id numbers 1 to 8 refer to poles drawn in Fig. 7. NCB (SCB): North (South) China Block, ELKB: Eastern Liaoning-Korea Block [54].

tions, although it is always situated on the far side of the distributions of poles. In the hypothesis of rigid continental blocks, we may propose an alternative interpretation, where our single pole is consistent with other Amuria and China poles and its far-sided position is due to an insufficient averaging of paleosecular variation.

Notwithstanding this limitation, we note that our pole is not inconsistent with the Gobi pole #14 (based on 30 specimens) of Pruner [50] and the Inner Mongolia pole (based on 6 sites) of Zhao et al. [16] (poles 4 and 5 respectively in Fig. 9b), and the Chulut Tsagan Del poles #12 (17 specimens) and #13 (19 specimens) of Pruner [50] exhibit a significant counterclockwise rotation (poles 2 and 3 respectively in Fig. 9b). Because three of these poles are based on only a few specimens, we may also question their effectiveness in averaging paleosecular variation, a possibility not discussed by the authors. We therefore attempt to define a new average Cretaceous paleopole for Amuria, including our Khurmen Uul pole and previously published ones, thus including data from 5 distinct localities within the Amuria block. Assuming that the rotations of Chulut Tsagan Del poles #12 and #13 are due to tectonic local rotations about a vertical axis (Fig. 9b), we computed a mixed average of small-circles passing through these poles and the other fixed poles (Khurmen Uul, Inner Mongolia, and Gobi #14). This average is an extension of the combined statistics of McFadden and McElhinny [39] to the case of populations of small-circles and vectors, as proposed by Enkin [51]. This mean pole lies at $\lambda = 77.3°$N, $\phi = 215.2°$E ($n = 5$, $A_{95} = 7.5°$). Indeed, this Amuria pole does not differ significantly from the China mean pole in terms of paleolatitudes ($\Delta\lambda = 1.2° \pm 3.0°$), and shows no rotation ($-4.0° \pm 5.1°$). Compared to the 90 Ma pole from the Eurasia APWP, this new Amuria pole exhibits an insignificant offset of $\Delta\lambda = 3.8° \pm 4.2°$, with no rotation ($5.2° \pm 7.3°$).

In conclusion, we reach two different interpretations, depending on whether or not the paleosecular variation has been efficiently averaged by our sampling. In the first hypothesis, the far-sided position of Khurmen Uul pole would indicate a c.a. ~1000 km of northward convergence of west Amuria with respect to Siberia. This hypothesis is very similar to the one advocated for Tarim block by Chen et al. [10] but hardly supported by geologic evidence and models of Asia deformation (e.g. [1–3,52]). This interpretation vanishes if paleosecular variation has not been completely averaged. In the framework of our second hypothesis, incompletely averaged paleosecular variation, our new pole could be reasonably consistent with previously published poles from Amuria and China. Indeed, if such is the case, the generally admitted assumption that SCB, NCB, ELKB and Amuria formed a single entity since their late Jurassic–Early Cretaceous accretion to Siberia remains valid.

Acknowledgements

We wish to thank O. Tamurtogoo, G. Badarch and J. Badamgarav from Geological Institute of Mongolian Academy of Sciences, for efficient organization

and guiding in the field during 1999 expedition to Gobi Desert. We also thank V. Ivanov, from the Siberian Branch of Russian Academy of Sciences, who suggested Khurmen Uul locality, and provided geological maps. An early draft of this paper benefited from helpful comments and suggestions from S. Gilder, V. Courtillot, B. Carter-Stiglitz, F. Lagroix and two anonymous referees. This is contribution 2057 of IPGP.

References

[1] P. Tapponnier, P. Molnar, Active faulting and cenozoic tectonics of Tien Shan, Mongolia, and Baykal regions, J. Geophys. Res. 84 (1979) 3425–3459.
[2] P. Molnar, P. Tapponnier, Cenozoic tectonics of Asia: effects of a continental collision, Science 189 (1975) 419–426.
[3] P. Tapponnier, G. Peltzer, R. Armijo, On the mechanics of the collision between India and Asia, Geol. Soc. Spec. Publ. 19 (1986) 115–157.
[4] J.P. Avouac, Applications des méthodes de morphologie quantitative à la néotectonique: modèle cinématique des déformations actives en Asie Centrale, Paris VII, 1991.
[5] R.J. Enkin, Z. Yang, Y. Chen, V. Courtillot, Paleomagnetic constraints on the geodynamic history of the major blocks of China from the permian to the present, J. Geophys. Res. 97 (1992) 13,953–13,989.
[6] Y. Chen, V. Courtillot, J.-P. Cogné, J. Besse, Z. Yang, R. Enkin, The configuration of Asia prior to the collision of India: Cretaceous paleomagnetic constraints, J. Geophys. Res. 98 (1993) 21,927–21,941.
[7] S.A. Gilder, X. Zhao, R.S. Coe, Z. Meng, V. Courtillot, J. Besse, Paleomagnetism and tectonics of the Southern Tarim Basin, Northwestern China, J. Geophys. Res. 101 (1996) 22015–22031.
[8] N. Halim, J.P. Cogné, Y. Chen, R. Atasiei, J. Besse, V. Courtillot, S. Gilder, J. Marcoux, R.L. Zhao, New Cretaceous and Early Tertiary paleomagnetic results from Xining-Lanzhou basin, Kunlun and Qiangtang blocks, China: implications on the geodynamic evolution of Asia, J. Geophys. Res. 103 (1998) 21,025–21,045.
[9] S. Gilder, Y. Chen, J.-P. Cogné, X. Tan, V. Courtillot, D. Sun, Y. Li, Paleomagnetism of Upper Jurassic to Lower Cretaceous volcanic and sedimentary rocks from the western Tarim Basin and implications for inclination shallowing and absolute dating of the M-O (ISEA?) chron, Earth Planet. Sci. Lett. 206 (2003) 587–600.
[10] Y. Chen, H. Wu, V. Courtillot, S. Gilder, Large N-S convergence at the northern edge of the Tibetan Plateau? New Early Cretaceous paleomagnetic data from Hexi Corridor, NW China, Earth Planet. Sci. Lett. 201 (2002) 293–307.
[11] Y. Chen, J.P. Cogné, V. Courtillot, P. Tapponnier, X.Y. Zhu, Cretaceous paleomagnetic results from western Tibet and tectonic implications, J. Geophys. Res. 98 (1993) 17,981–17,999.
[12] Z. Yang, J. Besse, Paleomagnetic study of Permian and mesozoic sedimentary rocks from Northern Thailand supports the extrusion model for Indochina, Earth Planet. Sci. Lett. 117 (1993) 525–552.
[13] Z. Yang, V. Courtillot, J. Besse, X. Ma, L. Xing, J. Zhang, Jurassic paleomagnetic constraints on the collision of the north and South China blocks, Geophys. Res. Lett. 19 (1992) 577–580.
[14] N. Halim, V. Kravchinsky, S. Gilder, J.P. Cogné, M. Alexyutin, A. Sorokin, V. Courtillot, Y. Chen, A paleomagnetic study from the Mongol–Okhotsk region: rotated early Cretaceous volcanics and remagnetized sediments, Earth Planet. Sci. Lett. 159 (1998) 133–145.
[15] X. Ma, Z. Yang, L. Xing, The Lower Cretaceous reference pole for north China, and its tectonic implications, Geophys. J. Int. 115 (1993) 323–331.
[16] X. Zhao, R.S. Coe, Y. Zhou, H. Wu, J. Wang, New paleomagnetic results from northern China: collision and suturing with Siberia and Kazakstan, Tectonophysics 181 (1990) 43–81.
[17] X. Zhao, R.S. Coe, Paleomagnetic constraints on the collision and rotation of North and South China, Nature 327 (1987) 141–144.
[18] S. Gilder, V. Courtillot, Timing of North-South China collision from new middle to Late Mesozoic paleomagnetic data from the North China Block, J. Geophys. Res. 102 (1997) 17,713–17,727.
[19] Z. Yang, J. Yin, Y.I. Otofuji, K. Sato, Discrepant Cretaceous paleomagnetic poles between Eastern China and Indochina: a consequence of the extrusion of Indochina, Tectonophysics 334 (2001) 101–113.
[20] Z. Yang, J. Besse, New Mesozoic apparent polar wander path for south China: tectonic consequences, J. Geophys. Res. 106 (2001) 8493–8520.
[21] V.A. Kravchinsky, J.P. Cogné, W. Harbert, M.I. Kuzmin, Evolution of the Mongol–Okhotsk ocean with paleomagnetic data from the suture zone., Geophys. J. Int. 148 (2002) 34–57.
[22] L.P. Zonenshain, M.I. Kuzmin, L.M. Natapov, Geology of the USSR: a Plate-Tectonic Synthesis, American Geophysical Union, Washington, D.C., 1990, 242 pp.
[23] T.L. Barry, R.W. Kent, Cenozoic magmatism in Mongolia and the origin of Central and East Asian basalts, in: M.F.J. Flowers, S.L. Chung, C.H. Io, T.Y. Lee (Eds.), Mantle Dynamics and Plate Interactions in East Asia, Geodynamics, vol. 27, American Geophysical Union, 1998, pp. 347–364.
[24] B.F. Windley, M.B. Allen, Mongolian plateau: evidence for a late Cenozoic mantle plume under central Asia, Geology 21 (1993) 295–298.
[25] W.D. Cunningham, B.F. Windley, D. Dorjnamjaa, G. Badamgarav, M. Saandar, Late Cenozoic transpression in southwestern Mongolia and the Gobi Altai-Tien Shan connection, Earth Planet. Sci. Lett. 140 (1996) 67–81.
[26] W.D. Cunningham, B.F. Windley, D. Dorjnamjaa, G. Badamgarav, M. Saandar, A tructural transect across the Mongolian Western Altai: active transpressional mountain building in central Asia, Tectonics 15 (1996) 142–156.

[27] W.D. Cunningham, B.F. Windley, L.A. Owen, B. Tiffany, D. Dorjnamjaa, J. Badamgarav, Geometry and style of partitioned deformation within a late Cenozoic transpressional zone in the eastern Gobi Altai Mountains, Mongolia, Tectonophysics 277 (1997) 285–306.
[28] W.D. Cunningham, Cenozoic normal faulting and regional doming in the southern Hangay region, Central Mongolia: implications for the origin of the Baikal rift province, Tectonophysics 331 (2001) 389–411.
[29] Y.A. Zorin, V.G. Belichenko, E.K.H. Turutanov, V.M. Kozhevikov, S.V. Ruzhentsev, A.B. Dergunov, I.B. Filippova, O. Tomurtogoo, N. Arvisbaatar, T. Bayasgalan, C. Biambaa, P. Khorsbayar, The South Siberia–Central Mongolia transect, Tectonophysics 225 (1993) 361–378.
[30] A.M.C. Sengor, B.A. Natal'in, V.S. Burtman, Evolution of the Altaid tectonic collage and Phanerozoic crustal growth in Eurasia, Nature 364 (1993) 299–307.
[31] V.S. Samoylov, V.G. Ivanov, M.M. Arakelyants, D.I. Frikh-Khap, V.V. Yarmolyuk, Late Mesozoic magmatism of the Arts Bogd region (Gobi Altai, Mongolia), Geol. Ser. 11 (1988) 14–26.
[32] J.J. Traynor, C. Sladen, Tectonic and stratigraphic evolution of the Mongolian People's Republic and its influence on hydrocarbon geology and potential, Mar. Pet. Geol. 12 (1995) 35–52.
[33] V.F. Shuvalov, Continental red bed of the Upper Jurassic of Mongolia, Dokl. Akad. Nauk. SSSR 189 (5) (1969) 1088–1091.
[34] J.F. Hicks, D.L. Brinkman, D.J. Nichols, M. Watabe, Paleomagnetic and palynologic analyses of Albian to strata at Bayn Shireh, Burkhant, and Khuren Duhk, eastern Gobi Desert, Mongolia, Cretac. Res. 20 (1999) 829–850.
[35] V.V. Yarmolyuk, V.G. Ivanov, V.S. Samoylov, M.M. Arakelianst, Formation stages of Mesosoic and Cenozoic intraplate volcanism of South Mongolia, Dokl. Akad. Nauk 344 (5) (1995) 673–676 (in Russian).
[36] J.D.A. Zijderveld, A.C. demagnetization of rocks: analysis of results, in: D.W. Collinson, K.M. Creer, S.K. Runcorn (Eds.), Methods in Paleomagnetism, Elsevier, New York, 1967, pp. 254–286.
[37] J.L. Kirshvink, The least-squares line and plane and the analysis of paleomagnetic data, Geophys. J. R. Astron. Soc. 60 (1980) 699–718.
[38] R.A. Fisher, Dispers. Sphere 217 (1953) 295–305.
[39] P.L. McFadden, M.W. McElhinny, The combined analysis of remagnetization circles and direct observations in paleomagnetism, Earth Planet. Sci. Lett. 87 (1988) 161–172.
[40] J.P. Cogné, PaleoMac: a Macintosh™ application for treating paleomagnetic data and making plate reconstructions, Geochem. Geophys. Geosyst. (2002) (Paris).
[41] J.G. Koenigsberger, Natural residual magnetism of eruptive rocks, Terr. Magn. Atmos. Elect. 43, 119–130 and 299–320, 1938.
[42] M. Le Goff, Lissage et limites d'incertitude des courbes de migration polaire; pondération des données et extension bivariate de la statistique de Fisher, C. R. Acad. Sci. Paris 311 (II) (1990) 1191–1198.
[43] R. Day, M. Fuller, V.A. Schmidt, Hysteresis properties of Titanomagnetites: grain-size and compositional dependence, Phys. Earth Planet. Inter. 13 (1977) 260–267.
[44] D.J. Dunlop, Theory and application of the Day plot (Mrs/Ms versus Hcr/Hc) 1. Theorectical curves and tests using titanomagnetite data, J. Geophys. Res. 107 (2002) 22.
[45] P.L. McFadden, A new fold test for paleomagnetic studies, Geophys. J. Int. 103 (1990) 163–169.
[46] J. Besse, V. Courtillot, Apparent and true polar wander and the geometry of the geomagnetic field over the last 200 Myrs, J. Geophys. Res. 107 (2002) 1–31.
[47] R.S. Coe, B.R. Globerman, P.W. Plumley, G.A. Thrupp, Paleomagnetic results from Alaska and their tectonic implications, in: D.G. Howell (Ed.), Tectonostratigraphic Terranes of the Circum-Pacific Region, Earth. Sci. Ser., vol. 1, Circum-Pac. Counc. for Energy and Miner. Resour, Houston, Tex., 1985, pp. 85–108.
[48] Y.A. Zorin, Geodynamics of the western part of the Mongolia–Okhotsk collisional belt, Trans-Baikal region (Russia) and Mongolia, Tectonophysics 306 (1999) 33–56.
[49] P.L. McFadden, R.T. Merill, M.W. McElhinny, L. Sunhee, Reversal of the Earth's magnetic field and temporal variations of the dynamo families, J. Geophys. Res. 96 (1991) 3923–3933.
[50] P. Pruner, Paleomagnetism and paleogeography of Mongolia from the Carboniferous to Cretaceous-final report, Phys. Earth Planet. Inter. 70 (1992) 169–177.
[51] R.J. Enkin, Formation et déformation de l'Asie depuis la fin de l'ère Primaire, Université Paris 7, 1990.
[52] J.P. Avouac, P. Tapponnier, Kinematic model of active deformation in Central Asia, Geophys. Res. Lett. 20 (1993) 895–898.
[53] D.V. Kovalenko, V.V. Yarmolyuk, A.V. Solov'ev, Migration of volcanic centers of the south Khangai hot spot : paleomagnetic evidence, GeoTectonics 31 (1997) 228–235.
[54] W. Lin, Y. Chen, M. Faure, Q. Wang, Tectonic implications of new Late Cretaceous paleomagnetic constraints from Eastern Liaoning Peninsula, NE China, J. Geophys. Res. 108 (2003) 1–17.